

## Circulation and turbulent exchange characteristics during the thermal bar in Lake Ontario

Yerubandi R. Rao,<sup>1</sup> Michael G. Skafel, and Murray N. Charlton

National Water Research Institute, 867 Lakeshore Road, Burlington, Ontario, Canada

### Abstract

We made observations from vertical moorings of thermistors and current meters in Lake Ontario to study the spring thermal bar circulation, its effect in inhibiting the horizontal mixing, and spatial and temporal variability of vertical mixing during this period. Thermal bar progression rates were compared with two analytical models; both produced overestimates during the early part of the thermal bar and underestimates during the late spring. In a zone between the shore and the thermal bar, currents were influenced by the local wind stress and flowed in a counterclockwise direction. The mean cross-shore flows in the nearshore zone were reduced during the thermal bar period. The alongshore horizontal exchange coefficients were higher than cross-shore exchange coefficients. During the thermal bar period, the magnitude of both alongshore and cross-shore exchange coefficients decreased when the bar was still within middepth (<40 m); when it was further offshore, the thermal bar did not have any significant effect on alongshore exchange coefficients, but cross-shore exchanges decreased marginally. The vertical exchange coefficients were high in the water column because of convective mixing during the thermal bar period. During the evolution of spring thermal bar, the vertical mixing decreased considerably in the nearshore regions under stable stratification, whereas the high vertical mixing levels continued in the offshore region for a longer period.

During early spring, the temperature in a large temperate lake is more or less constant and is <4°C (temperature of maximum density). As spring heating proceeds, the water is heated convectively, leading to a faster increase of temperature in shallow areas compared to deeper waters. When the temperature reaches 4°C, a stable stratification develops at the shore. Between this region and deep part of the lake that still experiences convection and a temperature below 4°C, there is a zone of sinking water in the vicinity of a temperature that corresponds to maximum density. This zone is referred to as the “thermal bar.” Some authors have also referred to the 4°C isotherm as the thermal bar (Farrow 2002). The thermal bar moves progressively toward the deepest part of the lake, until it finally disappears as summer stratification develops throughout the lake. The thermal bar phenomenon regularly occurs in the Great Lakes (Rodgers 1968) and other large lakes (Thikhomirov 1963; Malm et al. 1994). The duration of the thermal bar in these large lakes is ~1–2 months. The thermal bar is important because of its role in inhibiting the horizontal exchange of water between the nearshore and offshore regions (Gbah and Murthy 1998). This phenomenon is likely to affect physical, chemical, and biological characteristics and may lead to water pollution problems in the nearshore zone. Entrapment of the water on

the nearshore side has been indicated in some studies. Moll et al. (1993) observed high plankton productivity and locally abundant fish populations that were associated with the thermal bar overturning circulation.

Several analytical and numerical models describing density-induced circulation have been developed (Bennett 1971; Elliott 1971; Malm 1995). These studies concentrated on studying either the progression of the thermal bar (Elliott and Elliott 1970; Zilintinkevich et al. 1992) or understanding the circulation system associated with the thermal bar (Huang 1972; Farrow 1995; Gbah et al. 1998). The density-induced horizontal circulation in large temperate lakes of the northern hemisphere is counterclockwise in the stably stratified nearshore region and clockwise in the deep water region. Secondary circulation, which is perpendicular to primary circulation, consists of two circulation cells, one on each side of 4°C isotherm, where waters mix and descend. Ecosystem models for the thermal bar period have clearly shown that biological and chemical distributions are controlled by the interaction of circulation and mixing on either side of 4°C isotherm (Scavia and Bennet 1980; Botte and Kay 2000). There have been a number of field investigations of the thermal bar in the Great Lakes (Rodgers 1971; Csanady 1974; Moll et al. 1993) and in other large lakes (Thikhomirov 1963). These studies confirmed the general features of the temperature distribution in the thermal bar zone. However, except for a few studies (Malm et al. 1993), the simultaneous observations of currents and temperature measurements have been rarely reported. Even these observations are limited to a few surveys during the development phase of the thermal bar. Satellite data have been used in conjunction with field experiments to determine the surface water temperature (Malm et al. 1994).

Despite the past field investigations and the numerical models of spring circulation in large dimictic lakes, much remains unknown about this feature. As was mentioned earlier, the inhibiting nature of the bar has been observed in

<sup>1</sup> Corresponding author (Ram.Yerubandi@ec.gc.ca).

### Acknowledgments

We thank William Schertzer for useful discussions and his help in calculating the surface fluxes. Helpful comments by Joakim Malm (Lund University) are gratefully acknowledged. We also thank two anonymous reviewers for helpful comments that improved the manuscript. NWRI Engineering services and Technical Operations supported us in deploying and retrieving the moorings. Jacqui Milne and Tina Mamone are responsible for the field surveys.

Financial support for this work was provided by the Ontario Water Works Research Consortium.

Lake Ontario from the reduction of horizontal exchange coefficients (Gbah and Murthy 1998). However, these observations are limited to only one subsurface (10 m) level; therefore, the vertical distribution of horizontal exchanges is not available during the thermal bar period. In addition to horizontal mixing, numerical studies have also shown the variability of vertical mixing from stably stratified coastal areas to the deeper convective areas, with enhanced mixing near the 4°C isotherm. However, to our knowledge, the temporal and spatial variability of the vertical mixing during the evolution of the thermal bar has not been reported from these observations. The effect of winds on the circulation during the thermal bar has been found to be very important in numerical studies (Malm 1995), and this needs to be verified in field experiments. It is therefore particularly important to be able to analyze the experimental evidence in detail, to determine the importance of exchange processes and the overall circulation during the thermal bar period.

Because of these concerns and the renewed issue of abundant *Cladophora* sp. fouling beaches each summer in Lake Ontario, a multidisciplinary team has been formed by the National Water Research Institute to address these issues. One aspect that is being studied is the development of the algae early in the spring. It is postulated that there may be a significant opportunity for vigorous growth during the spring evolution of the thermal bar. The data collected during spring 2003 offer the opportunity to perform a detailed analysis of circulation and mixing during the spring thermal bar in Lake Ontario. The present article presents detailed measurements of the time series of current and temperature profiles from several moorings and weekly water quality surveys from a research vessel. The purpose of the research is to study the spring circulation during the evolution of the thermal bar. It also provides an opportunity to quantify the vertical distribution of horizontal exchanges and vertical mixing as the thermal bar progresses in Lake Ontario.

## Materials and methods

**Experimental data**—The measurements for obtaining currents, winds, and temperatures consisted of Eulerian measurements during the spring of 2003. As part of the field program, current meter and thermistor moorings were deployed at a cross-section off Oakville in the western end of Lake Ontario (Fig. 1). The reasons for selecting this region were (1) the coastline is more or less straight, with relatively simple bottom topography, and (2) this area is known to be affected by attached algae (*Cladophora*) from early spring to summer. The local bathymetry has a gentle slope, with depths of 10 m at 0.9 km from shore to 80 m at 8.9 km from shore. The mooring setup was designed to capture the onshore-offshore flow structure at fixed points along an axis that is more or less perpendicular to the local shore line. Three broadband and one narrowband RDI Acoustic Doppler Current Profilers (ADCP) provided vertical profiles of horizontal currents during this period. The ADCP located at 21 m water depth (Sta. 22A) was mounted at the bottom, facing up. The rest of the ADCPs were installed at a depth of 15–16 m below the surface on stable subsurface floats facing

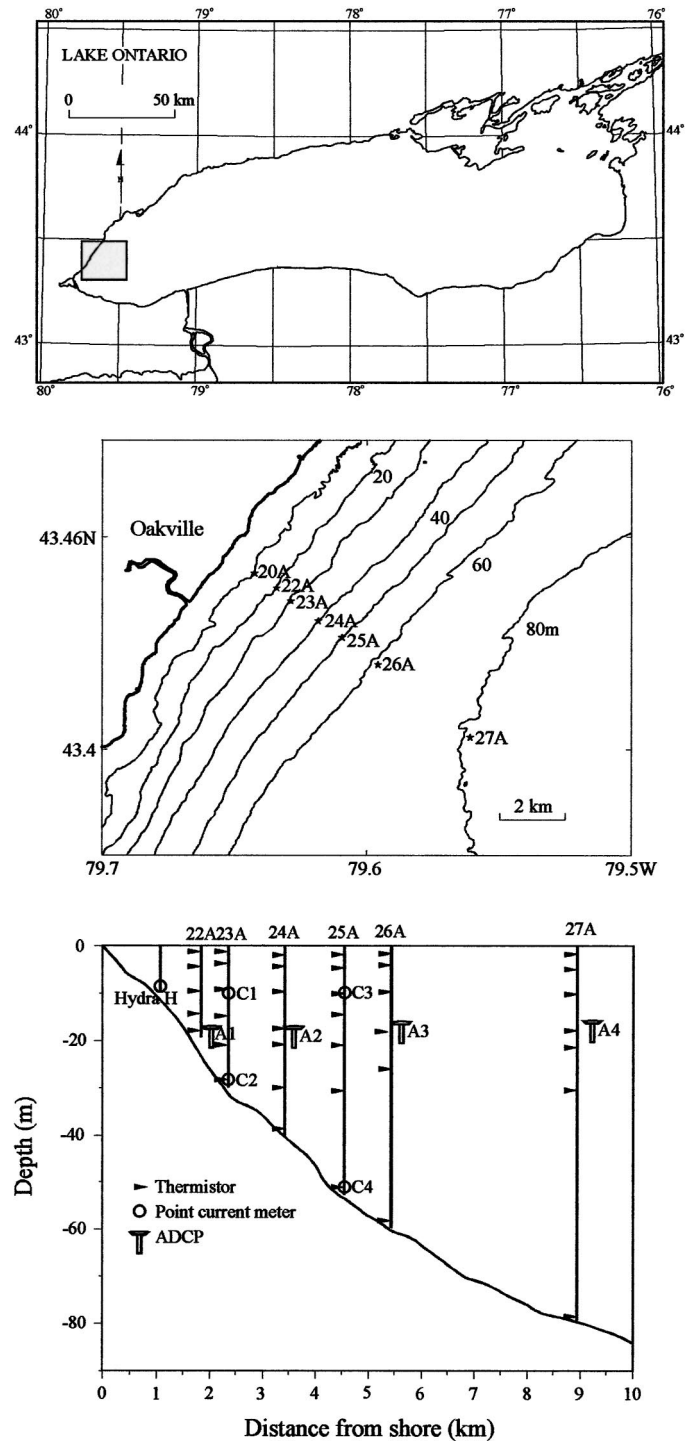


Fig. 1. Map of Lake Ontario with experimental setup, local bathymetry, and instrument configuration.

up. Measured vertical resolution was set at a 1-m bin interval. In addition to ADCPs, single-point current meters (Nobska MAVS) at subsurface (10 m) and 1 m above the bottom were deployed at two locations. The accuracy of all these measurements is of considerable significance in the analysis. The current speed measurements are accurate to the order of  $0.3 \text{ cm s}^{-1}$  for MAVS and  $0.25 \text{ cm s}^{-1}$  for ADCPs, whereas

directions are accurate to  $\pm 2^\circ$  for both types of instruments. The data return of currents from ADCPs was excellent; however, the data from MAVs were not complete because of the directional problems encountered in the deployment. In the shallow region at 11-m depth, a current measuring system, Sontek-Hydra, was deployed. Unfortunately, this system did not function for the whole deployment period.

Water temperature data were obtained from six moorings with thermistors deployed at 5-m intervals in the epilimnion and at a lesser frequency (10 m) in the bottom waters. Apart from this, water temperature was also obtained from the current meters and the ADCP instrument location at the bottom. The different temperature sensors used in the experiment yielded an accuracy of temperature of  $\pm 0.002\text{--}0.2^\circ\text{C}$ . A land-based meteorological station at the western end of the lake provided the wind and radiation data from days 119 (29 April) to 171 (20 June). The incoming and net radiations were measured with an Eppley pyranometer and a net radiometer. The radiation budget terms by this method can be measured to an accuracy of 5% of the measured value. The wind data from Toronto island airport, which is  $\sim 20$  km from the experimental site, were substituted for the missing data from days 91 (1 April) to 118 (28 April). No radiation data were available from this station during this period.

The experiment also consisted of several weekly surveys measuring the water quality parameters from a research vessel during the thermal bar evolution. Each survey consisted of measuring temperature, conductivity, and chlorophyll at nine stations in the same cross-section off Oakville using an YSI water quality profiler in the experimental region. Samples for water chemistry were collected at 1 m depth at all nine stations.

**Meteorological observations**—A low-pass filter, using an 8-h period for the cutoff, was used to remove the high-frequency information in the wind speed and direction (Fig. 2a). The filtered time series had peaks of  $>10\text{ m s}^{-1}$  during the early part of spring (days 91–110), which were usually associated with easterly storms. The winds were moderate during the rest of the experimental period, except on day 132. On that day, strong westerly winds ( $\sim 15\text{ m s}^{-1}$ ) blew over the experimental region. The assumption that the wind is evenly distributed over the surface of the lake must be considered to be approximate only. However, the wind events that have strong influence on the progression of the thermal bar are mainly associated with storms moving along the lake, which will have a more or less uniform wind field in this region.

The surface heat flux ( $Q_T$ ) was calculated as a balance between the heat sources and sinks,

$$Q_T = Q\downarrow + Q\uparrow - Q_h - Q_e \quad (1)$$

The total incoming radiation ( $Q\downarrow = K\downarrow + L\downarrow$ ) was obtained from the instrument output of the radiometer ( $Q$ ) and the temperature of blackbody cavity ( $T_{\text{cav}}$ ) by  $Q\downarrow = Q + \sigma T_{\text{cav}}^4$ , where  $\sigma$  is Stephen-Boltzmann constant. Here  $K\downarrow$  and  $L\downarrow$  are incoming solar radiation and incoming longwave radiation, respectively. Because  $K\downarrow$  was available from the pyranometer, we can obtain the longwave radiation by the difference (i.e.,  $L\downarrow = Q\downarrow - K\downarrow$ ). Average incoming long-

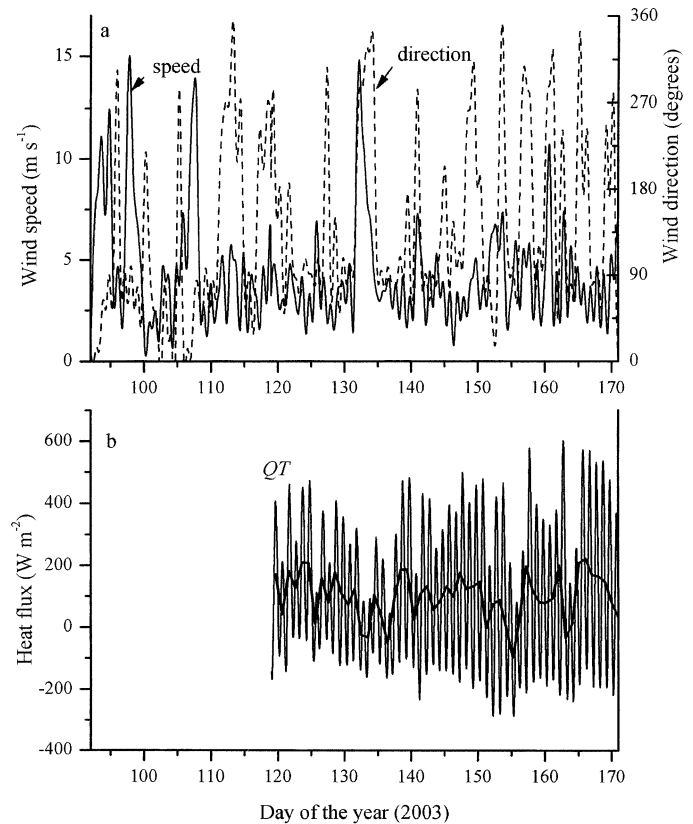


Fig. 2. Time series of (a) low-pass filtered ( $>8$  h) wind speed and direction and (b) surface heat flux,  $Q_T$ . The thick line indicates the daily averaged value.

wave radiation increases during the spring period and reaches a maximum value during the summer. Furthermore, the reflected solar radiation was obtained as  $K\uparrow = \alpha K\downarrow$ , where the surface albedo ( $\alpha$ ) was assumed as 0.08 on the basis of previous experience in Lake Ontario (Davies et al. 1975). The reflected longwave radiation is a small component of the radiation balance, and  $L\uparrow$  was obtained as  $(1 - \epsilon)L\downarrow$ , where  $\epsilon$  ( $=0.97$ ) is the emissivity of the water surface (Schertzer 1987). Finally, the total outgoing radiation was obtained as ( $Q\uparrow = K\uparrow + L\uparrow$ ). All radiation instruments were routinely calibrated before field installation. Sensible ( $Q_h$ ) and latent ( $Q_e$ ) heat fluxes were calculated as described in Schertzer (1987). Figure 2b shows the hourly (thin curve) and daily averaged (thick curve) surface heat flux during the experimental period. The daily averaged heat flux ranged from  $-98.3$  to  $221\text{ W m}^{-2}$  during the spring. Significant nearshore-offshore gradients in the net heat flux are expected during the spring because of intense warming and wind-induced upwelling and downwelling events during late spring. However, the wind data showed that, during the major part of the thermal bar evolution, winds were moderate except during a westerly storm, and hence would not have favored intense turbulent heat and mass exchanges at the air-water interface. Also, the temperature structure, which will be discussed later, did not show major upwelling/downwelling events, except for the event on days 132–133. Therefore, the

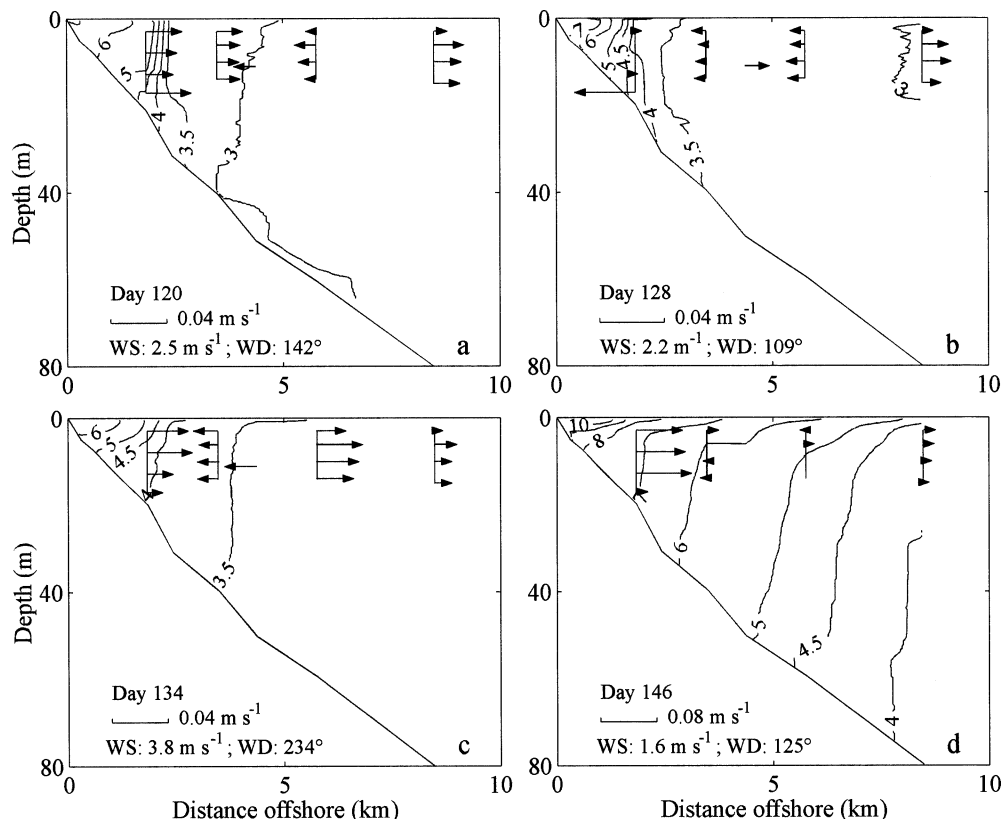


Fig. 3. Measured temperature (in °C) distributions along the cross-section off Oakville from vessel surveys on (a) 30 April (day 120), (b) 8 May (day 128), (c) 14 May (day 134), and (d) 26 May (day 146). The average wind speed (ws), wind direction (wd), and current profiles for the survey period are shown in each figure.

heat flux observations from this coastal station can be considered to be representative for the analysis area.

*Spatial distribution of temperature*—The water quality surveys were carried out on 10, 24, and 30 April; 8, 14, and 26 May; and 3 and 10 June of 2003. The duration of a typical survey could be ~3–4 h. Although all of the surveys are complete (a total of nine stations occupied), we present the temperature data for four selected surveys during this period. Figure 3a–d shows the temperature structure for days 120 (30 April), 128 (8 May), 134 (14 May), and 146 (26 May), respectively. The corresponding wind speed and direction averaged over the survey period are inserted in the plots. The mean cross-shore currents (averaged over each survey) were plotted at selected depths. By day 120, the thermal bar was well developed, and the 4°C isotherm was present 2.2 km from the shore. Weak stratification was noticed in the nearshore zone. As was observed by Rodgers (1971) the horizontal temperature gradients near the 4°C isotherm were large compared with the regions away from it. This could be due to the mixing associated with downwelling circulation in the vicinity of the thermal bar. The mean cross-shore currents on days 128 and 134 indicate that the currents were converging near the 4°C isotherm in the surface levels. However, on day 120, the cross-shore currents flowed in the offshore direction near the thermal bar region.

The thermal bar was stationary in this area for the next two weeks, which can be observed from the 4°C isotherm on day 134. The temperature structure of the nearshore zone shows that the westerly storm on days 132–133 caused coastal upwelling. This can be clearly seen from the reduction in nearshore temperatures by 1°C and tilting of the isotherms between 4°C and 5°C. The westerly storm and the subsequent calm weather with positive heat flux significantly increased the speed of progression of the thermal bar to the deeper regions, as seen by the data for day 146. The 4°C isotherm can be seen ~8 km from the shore. A stable stratification developed in the nearshore zone.

## Results

*Temporal distribution of temperature*—Figure 4a–d shows the vertical temperature distribution at four selected thermistor moorings. The data were filtered with an 8-h low-pass filter to remove the high-frequency fluctuations. The thermal bar was seen as a shaded region when the water at 4°C was observed throughout the water column. Although, as had been observed in previous investigations, the bar migration was progressive, exceptions were observed on a few occasions. For instance, at 20 m water depth (Sta. 22A), the 4°C isotherm over the depth first appeared on day 114, but the water became cooler (3.5°C) from day 115.5 to 118. The

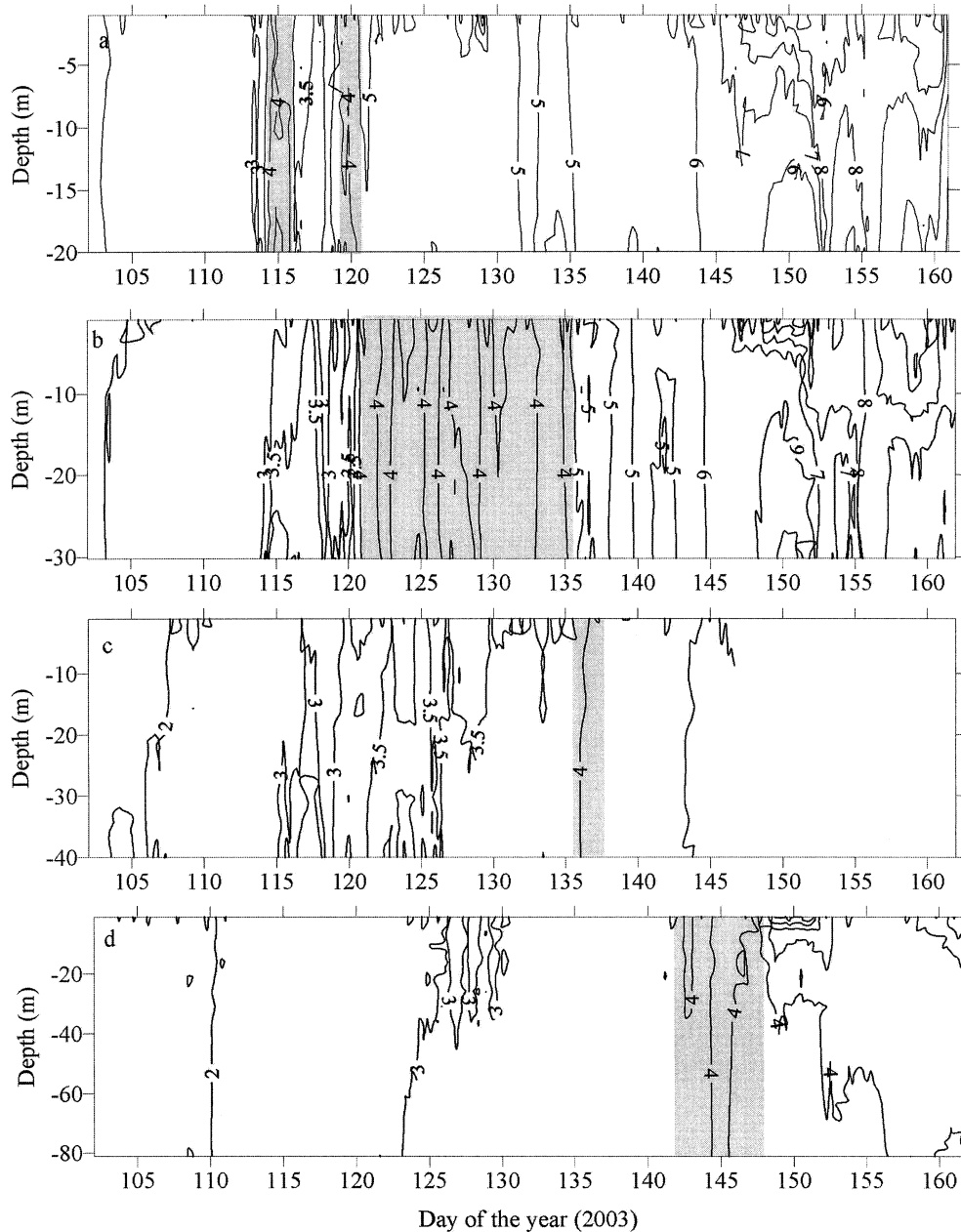


Fig. 4. Time series of low-pass filtered (>8 h) vertical temperature distributions at four stations: (a) 22A, (b) 23A, (c) 24A, and (d) 27A. The local thermal bar periods are identified as shaded regions in each figure.

surface heat-flux data were not available during this period, but because no weather system traveled over the lake during this period, it is reasonable to assume that weak upwelling along the northern shore would have lowered the temperatures to  $<4^{\circ}\text{C}$ . The winds during this period were moderate westerly winds, which could have caused the onshore transport from deeper waters. The thermal bar reappeared on day 119 and was present at this location until day 120. As was mentioned above, the thermal bar was stationary for 2 weeks, on days 121–135, 2.35 km (Sta. 23A) from the shore. The positive heat flux before the westerly storm on days 132–133 increased the stratification in the nearshore zone,

as seen in Fig. 4a and the shipboard survey on 8 May (Fig. 3b). The westerly storm seems to have been responsible for the quick offshore migration of the thermal bar beyond Sta. 23A.

The relative importance of wind-driven and density-induced currents in the vicinity of the thermal bar for different wind and horizontal temperature stratification conditions can roughly be estimated by comparing the wind force at the surface with the pressure force due to horizontal temperature gradient. According to the method of Malm (1995), the wind force at the surface of the water column is  $F_w = C_D \rho_a W^2$ , and the pressure force can be written as  $F_p = \int_{-D}^0 -(\partial p / \partial y)$

$dz$ . By assuming vertically well-mixed conditions and neglecting the pressure gradient due to the sloping of the water surface, the pressure gradient due to the horizontal density gradients can be expressed as  $F_p = -(1/2)(\partial\rho/\partial y)gD^2$ . Here, the drag coefficient  $C_D = 1.3 \times 10^{-3}$ ,  $\rho_a$  is the density of air ( $1.2 \text{ kg m}^{-3}$ ),  $W$  is the wind velocity,  $g$  is the acceleration due to gravity, and  $D$  is the depth at the location of the thermal bar. The horizontal density gradient ( $\partial\rho/\partial y$ ) was obtained from temperature measurements between Sta. 22A and 23A. The freshwater density was obtained using the formula of Chen and Millero (1986). During the stationary phase of the thermal bar on days 121–132 at Sta. 23A, the ratio of the pressure force to the wind force ( $F_p/F_w$ ) varied from 0.6 to 1.8, indicating that wind-driven circulation was an important factor during this period. However, the strong westerly wind event on day 132 has decreased the ratio to 0.015, indicating the dominance of wind-driven circulation over the density-induced circulation.

From the time series of temperature observations, the progression rate of the thermal bar can be estimated as the ratio of bar displacement from one mooring location to the other. Elliott and Elliott (1970) showed by an analytical model that the main factors controlling the progression of the thermal bar are surface heat flux and bottom topography. The model assumes that horizontal heat fluxes are of secondary importance and that complete vertical mixing results from convection in the unstably stratified region. In this model, the surface heat flux is considered to be constant in space and time distributed over the local depth. The temperature distribution in the region with water temperatures  $\leq 4^\circ\text{C}$  is then described by

$$T(x, t) = T_o(x) + \frac{Q_T(t - t_o)}{\rho_w C_p D(x)} \quad (2)$$

where  $t$  is time,  $T$  is temperature,  $T_o(x)$  is the initial temperature distribution at  $t_o$ ,  $Q_T$  is the surface heat flux,  $\rho_w$  is the freshwater density,  $C_p$  is the specific heat of water, and  $D(x)$  is the depth at distance  $x$  from the shore. The position of the thermal bar  $x = l$  can be obtained by inserting  $T(l) = T_m = 4^\circ\text{C}$  into Eq. (2).

Malm et al. (1993) approximated the initial temperature distribution  $T_o(x) = T_m - (\partial T/\partial x)_0(x - l_o)$  and  $D(x) = D_o + \mu(x - l_o)$ . This leads to the expression for thermal bar position

$$l(t) = l_o - \frac{D_o}{2\mu} + \sqrt{\left(\frac{D_o}{2\mu}\right)^2 + \frac{Q_T(t - t_o)}{\rho_w C_p \mu (\partial T/\partial x)_0}} \quad (3)$$

where  $D_o$  is the depth at the initial position of the thermal bar at  $l = l_o$ ,  $(\partial T/\partial x)_0$  is the initial horizontal temperature gradient in the cold zone, and the bottom slope  $\mu$  is taken to be constant in the horizontal direction.

The model by Zilitinkevich et al. (1991) incorporated the horizontal heat flux near the thermal bar zone into their analytical model, which is given by

$$\left\{ \left( \frac{\partial T}{\partial x} \right)_0 (l - l_o) - \frac{Q_T(t - t_o)}{\rho_w C_p [D_o + \mu(l - l_o)]} \right\} \frac{dl}{dt} = F_l \quad (4)$$

where  $F_l$  represents the vertically averaged horizontal dy-

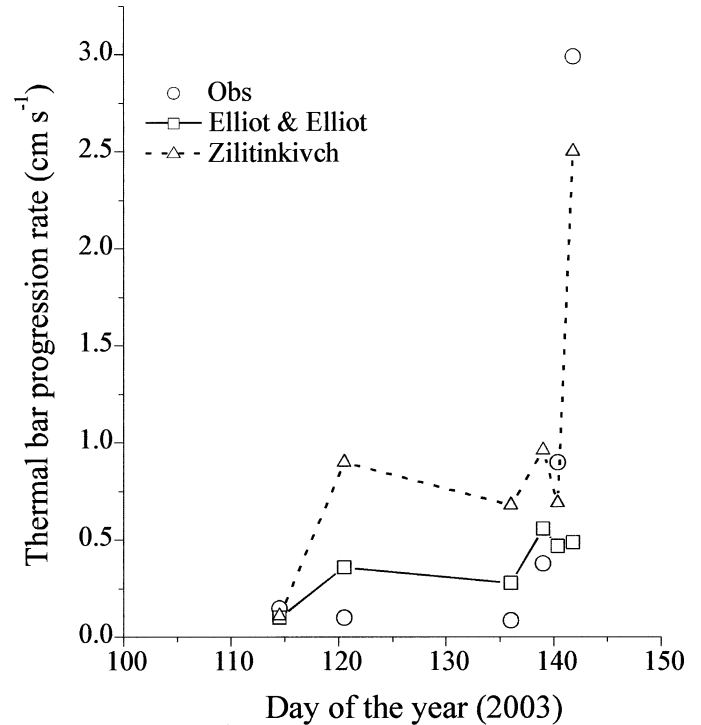


Fig. 5. Thermal bar progression rates from the observations and model results.

namical heat flux through the vertical  $x = l$ , given as  $F_l = C_l(ga\mu l)^{1/2}(T_w - T_m)^2$ . Here  $C_l = 0.03$ ,  $T_m$  is the temperature of maximum density, and  $T_w$  is the temperature averaged over the warm zone. Malm et al. (1993) solved the two-dimensional heat transfer equation for obtaining the temperature of the warm zone. However, we calculated  $T_w$  from the hourly time series of temperature observations from the thermistor moorings in the warm zone. The hourly  $T_w$  values are provided as input for calculating the dynamical heat flux. The initial conditions for Eq. (4) are  $l = l_o$  at  $t = t_o$ .

Figure 5 shows the comparison of model predictions and observations. The observed progression speed of the thermal bar indicates an initial slow phase and a later fast phase. This two-phase propagation of the thermal bar was also observed in the laboratory experiments of Elliott and Elliott (1970) and Kreyman (1989). Farrow (1995) attributed this relatively slow propagation of the thermal bar in the early phase to inertia of the existing flow. The model predictions using average heat fluxes during the integration period seem to be reasonable during the formation of the thermal bar in the shallow region (within a 20-m depth contour). However, both models overestimated the thermal bar progression rates from days 120–139 and underestimated it thereafter. The model of Zilitinkevich et al. (1991) significantly overestimated progression rates in the early phase of the thermal bar development but were able to predict the significant increase in the progression rate toward the end of the experiment. This indicates that the inclusion of mixing in the bar zone is important; however, both models failed to predict the stationary phase of the thermal bar. The discrepancies between model results and observations are probably due to wind-

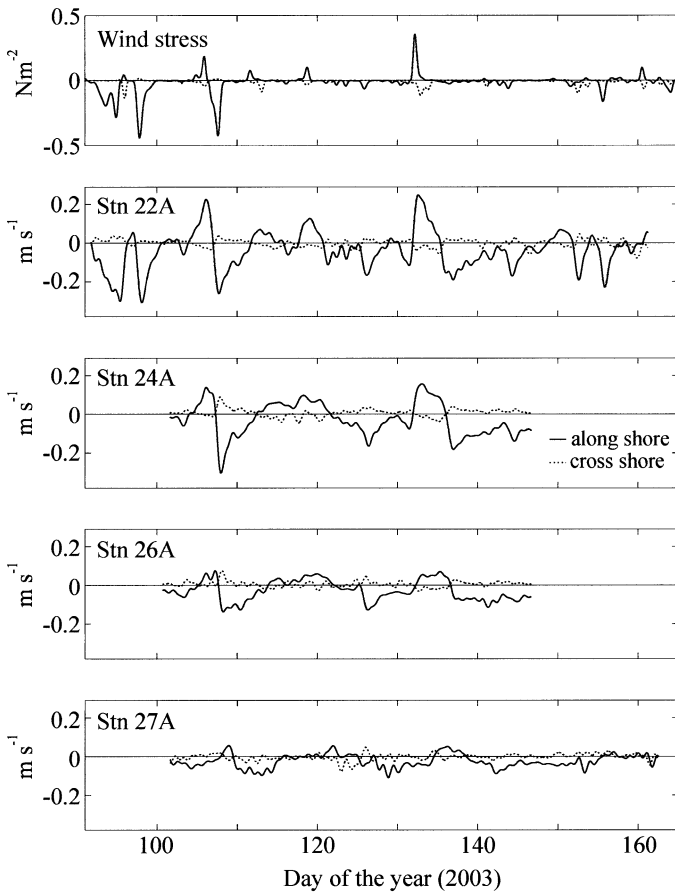


Fig. 6. Time series of low-pass filtered (24 h) alongshore (positive to the east) and cross-shore (positive to onshore) components of (a) wind stress and depth-mean currents at four ADCP stations.

driven currents and the use of average heat fluxes in the models or, possibly, that the models are two-dimensional and do not take alongshore effects into consideration. The prevailing winds, particularly the stronger events, seem to be a major factor in determining the progression rates in this part of the lake. From satellite pictures, it was observed that the thermal bar had disappeared in the western basin by day 150. However, cooler waters ( $<4^{\circ}\text{C}$ ) prevailed until the middle of June in the central and southeast basins of Lake Ontario (figures not shown).

**Circulation characteristics**—From the temperature distributions described above, the thermal distribution is affected strongly not only by the heat fluxes but also by the prevailing winds. Several studies in Lake Ontario have clearly shown the importance of alongshore wind stress on the nearshore circulation (Gbah and Murthy 1998). The alongshore and cross-shore components of currents and winds are obtained by rotating the east and north components by  $50^{\circ}$  counter-clockwise. The time series of winds and currents have been low-pass filtered (24 h) to remove the diurnal and inertial oscillations from the data. Figure 6 presents time series of low-pass filtered alongshore and cross-shore components of wind stress and mean currents from all bins of the respective ADCP. The wind stress was calculated by a quadratic for-

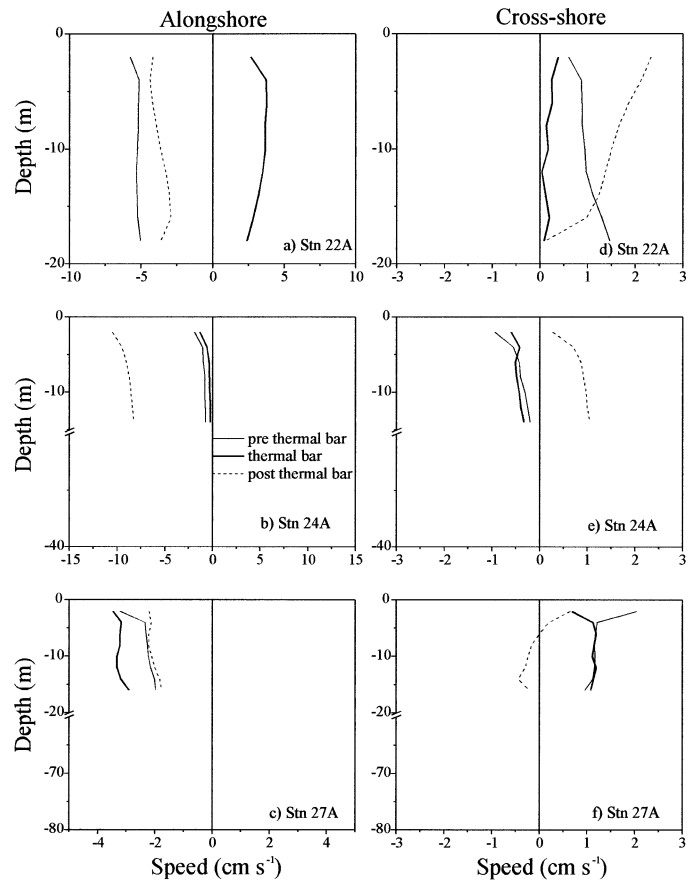


Fig. 7. Depth variation of mean alongshore and cross-shore currents during the pre-thermal bar, thermal bar, and post-thermal bar periods at stations (a) 22A, (b) 24A, and (c) 27A.

mula described in Rao and Murthy (2001). Time series of currents also show the flow reversals associated with the prevailing winds. The figures show that the alongshore currents within 6 km from the shore responded well to the alongshore wind stress. The currents at the offshore station (27A) showed that they are oppositely directed by strong easterly winds, whereas they are more or less in the same direction by westerly winds. During the easterly wind episodes, the nearshore currents responded immediately and flowed toward the west; however, in deeper waters, the currents responded to the wind forcing with a lag of a few hours. As was discussed earlier, on days 115.5–118, surface currents also showed that the temperature decreased in the nearshore regions due to upwelling caused by moderate westerly winds. The strong response of the westerly storm on currents on day 132 can be clearly seen from the figures. During this period, surface currents were predominantly eastward and in the offshore direction. The currents from the bottom bins of ADCPs (Sta. 24A and 26A) show that the mean transport was toward the shore (figures not shown). As was discussed, earlier this upwelling event seems to have had a significant effect on the progression of the thermal bar.

Figure 7a–f shows the depth variation of mean values of alongshore and cross-shore components of the currents at three selected ADCP stations. The time series is broken into

three parts—the pre-thermal bar, thermal bar, and post-thermal bar periods—at each station. In the shallow zone at Sta. 22A during the pre-thermal bar (days 100–114.5), and post-thermal bar (days 120–160) periods, the mean alongshore currents were toward the west. The mean alongshore currents during the thermal bar period were comparatively weak ( $\sim 2.5 \text{ cm s}^{-1}$ ) and were toward the east. A significant variability in cross-shore velocities were also observed from the thermal bar period to the pre- and post-thermal bar seasons. It can be seen that the onshore flow toward the bottom during the pre-thermal bar period was larger than during the post-thermal bar period. At the middepth station (24A), the pre-thermal bar period was on days 102–134 and the post-thermal bar period was on days 137–147, whereas, at the offshore station (27A) the pre-thermal bar was on days 102–142 and post-thermal bar period was on days 147–161. The middepth (24A) and offshore (27A) stations show a slightly different picture than the coastal station. Here, the mean alongshore currents did not change direction during the thermal bar period; however, the mean cross-shore velocities showed offshore flow during the thermal bar period. In general, the mean cross-shore flow reduced during the thermal bar period.

The vertical structure of mean cross-shore currents presented in Fig. 3a–d show that surface currents on the near-shore side of the thermal bar were directed toward the thermal bar. This indicates a strong possibility of horizontal heat transport from nearshore areas toward offshore in the surface layer during the pre-thermal bar period. The horizontal heat transport along a section can be estimated by calculating the changes in heat content in water columns (Malm 1993). The change in heat content ( $\partial H/\partial t$ ) is caused by surface heating ( $Q_T$ ) and horizontal heat transport ( $HT$ ):

$$\frac{\partial H}{\partial t} = Q_T - HT \quad (5)$$

where  $H = \rho_w C_p \int_0^D T dz$ . To estimate the rate of change of heat content, we made use of hourly observations of temperature ( $T$ ) at all thermistor stations. As an example, from all the estimates made at Sta. 22A, 23A, and 24A when the thermal bar was at Sta. 25A indicates that the average magnitudes of ( $\partial H/\partial t$ ) and  $Q_T$  were  $84.43$  and  $106.5 \text{ W m}^{-2}$ , respectively. These computations indicate that there was net horizontal heat transport from nearshore areas to the thermal bar zone.

**Horizontal mixing**—To estimate the vertical structure of horizontal exchange coefficients, we used current velocity data obtained from the ADCP stations considered for the mean flow. The earlier study by Gbah and Murthy (1998) showed that, during the thermal bar period, a low-pass filter of 8–14 h revealed short-term fluctuations that were responsible for horizontal mixing. Typical plots of kinetic energy spectra of along-shore and cross-shore components (figures not shown) showed that the spectral energy levels at high frequency ( $>0.125 \text{ cph}$ ) were rather low (5% of total energy) and roughly indicated the turbulent fluctuations. Therefore, the time series of filtered ( $>8 \text{ h}$ ) flow values  $\bar{u}(t)$  and  $\bar{v}(t)$  are subtracted from the observed hourly values  $u(t)$  and  $v(t)$  to obtain the fluctuations  $u'(t)$  and  $v'(t)$ .

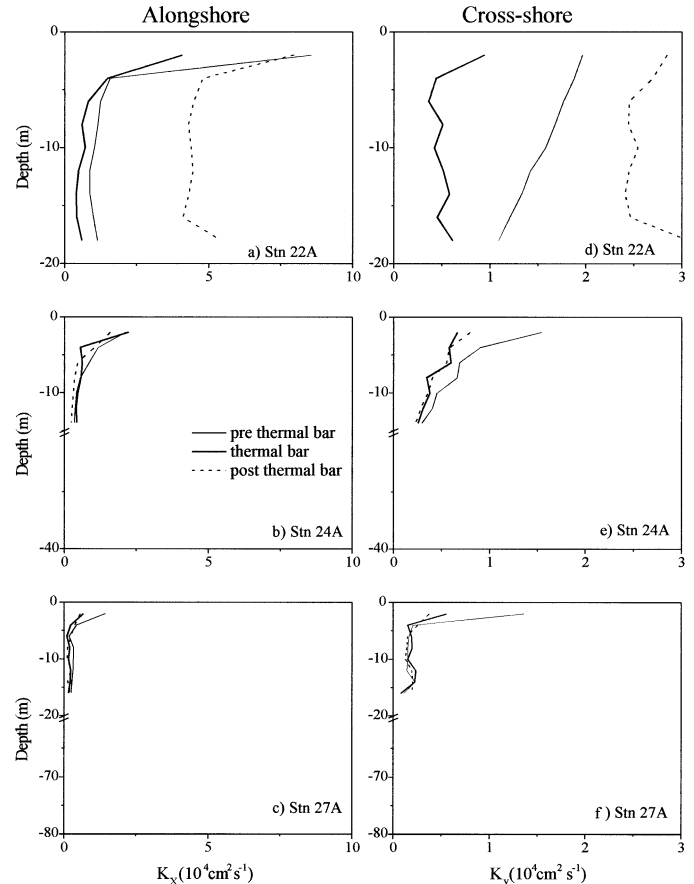


Fig. 8. Depth variation of horizontal exchange coefficients during the pre-thermal bar, thermal bar, and post-thermal bar periods at stations (a) 22A, (b) 24A, and (c) 27A.

By following Taylor's (1921) analysis, a relationship was developed between the horizontal exchange coefficient and the Eulerian current fluctuations in Lake Ontario (Rao and Murthy 2001). In that study, the horizontal exchange coefficients in terms of Eulerian statistics were written as  $K_x = \beta \overline{u'^2} \tau$ ,  $K_y = \beta \overline{v'^2} \tau$  where  $\tau = \int_0^\infty R(\tau) d\tau$  is the Eulerian integral timescale, and  $R(\tau)$  is the Eulerian autocorrelation coefficient and  $\beta = 1.4$ . As described in that study, the horizontal exchange coefficients obtained from this method are a reasonable estimate, given that our primary goal was not the precise quantification of the exchange coefficient but an estimate of horizontal mixing. Also, from a practical point of view, seasonal climatological characteristics of horizontal exchange coefficients during spring and their variability during thermal bar progression can be established from a long time series of current profiles under actual meteorological conditions. In contrast to the Gbah and Murthy (1998) study, as was described in the mean flow calculations, we obtained the exchange coefficients that were exclusively associated with the immediate area of the bar by considering the time series data at each ADCP station as the bar advances from that location. This approach was more effective because it considered the dynamic nature of the bar.

Figure 8a–f shows significant variability of horizontal exchange coefficients in the water column. It is clear from this

figure that the horizontal exchange coefficients are not isotropic over the depth in the coastal areas but become nearly isotropic in the offshore areas. At shallow depths, the along-shore exchange coefficients ( $K_x$ ) were higher in the surface layer ( $8.0 \times 10^4 \text{ cm}^2 \text{ s}^{-1}$ ) than subsurface values ( $1\text{--}5 \times 10^4 \text{ cm}^2 \text{ s}^{-1}$ ) during both the pre- and post-thermal bar periods. The magnitude of alongshore and cross-shore exchange coefficients considerably decreased during the thermal bar period. However, at the middepth and offshore stations, the thermal bar did not show a significant effect on alongshore exchange coefficients. The cross-shore exchange coefficients reduced slightly during the thermal bar and post-thermal bar periods at the middepth station. However, at the deeper station, the effect of the thermal bar in reducing the cross-shore exchange coefficients was confined to near the surface. In general, the horizontal exchange coefficients were higher in the nearshore areas than in the deeper regions. The general range of cross-shore exchange coefficients ( $0.1\text{--}0.6 \times 10^4 \text{ cm}^2 \text{ s}^{-1}$ ) during the thermal bar period was comparable to the results of the previous study by Gbah and Murthy (1998). Low values of horizontal exchange coefficients during the thermal bar period, compared with the pre- and post-thermal bar periods, support the hypothesis that the thermal bar plays an important role in suppressing the horizontal mixing.

**Vertical mixing**—Several mechanisms, such as current shear, breaking of internal waves, or convective overturns, contribute to the generation of vertical turbulence in lakes. The strong influence that the vertical shear and stability have on turbulence can be estimated from the gradient Richardson number,  $Ri = N^2/Sh^2$ . Here,  $N$  is the Brunt-Vaisala frequency, given as  $N^2 = -(g/\rho_0)(\partial\rho/\partial z)$  and the vertical current shear  $Sh^2 = (\partial u/\partial z)^2 + (\partial v/\partial z)^2$ , where  $z$  is the vertical coordinate positive upward,  $u$  and  $v$  are hourly alongshore and cross-shore currents, respectively,  $g$  is the acceleration due to gravity, and  $\rho_0$  is the reference density.

The turbulent mixing can be calculated on the basis of different models using advanced turbulence closure schemes. However, according to the method of Rao and Murthy (2001), we used a simple empirical formula suggested by Pacanowski and Philander (1981). They related the eddy viscosity to the Richardson number and studied the modeling of temperature structure in the tropical ocean, which is given as

$$K_z = \frac{K_o}{(1 + 5Ri)^2} + K_b \quad (6)$$

where  $K_o = 10^{-2} \text{ m}^2 \text{ s}^{-1}$  is an adjustable parameter, and  $K_b$  is the background eddy viscosity ( $=10^{-6} \text{ m}^2 \text{ s}^{-1}$ ). The density of the lake water was estimated from the temperature data from thermistor moorings and current meters and calculated according to the formula of Chen and Millero (1986). The temperature data at different levels were smoothly interpolated using a cubic spline technique, to match with ADCP current measurement levels.

Figure 9a–c shows the time series of vertical exchange coefficient at three ADCP stations. The comparison of wind stress (Fig. 6a) and vertical exchange coefficient showed that mixing in the surface mixed layer was closely related to alongshore wind stress. However, during the weak to mod-

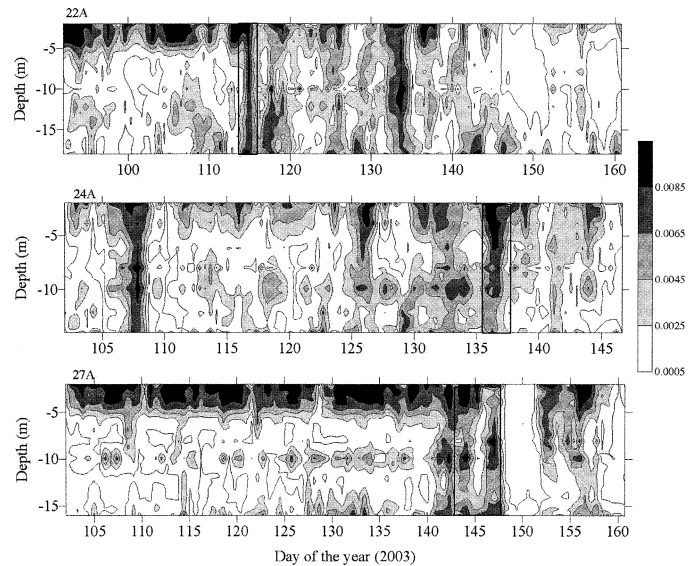


Fig. 9. Time series of the vertical exchange coefficient ( $\text{m}^2 \text{ s}^{-1}$ ) at stations (a) 22A, (b) 24A, and (c) 27A

erate winds, the effect of the thermal bar could be noticed. In Fig. 9a, on days 114.5–116 the vertical exchange coefficients increased significantly because of convective mixing during the thermal bar episode. Similar enhanced mixing could be seen on days 135.5–137 at Sta. 24A and days 142.5–147.5 at Sta. 27A. The current shear data (Fig. 7a–f) showed that shear did not significantly increase during the thermal bar period. However,  $N^2$  would have decreased because of convective mixing, which resulted in the increased vertical mixing. Because of low values of  $N^2$ , the Richardson numbers decreased to near critical values ( $<0.25$ ) in the water column, thus enhancing the turbulence. Part of this enhanced turbulence resulted in increased vertical exchange coefficients ( $0.0065\text{--}0.0085 \text{ m}^2 \text{ s}^{-1}$ ) during the thermal bar episode. The effect of stable stratification in reducing the vertical mixing could be clearly observed at the nearshore station (22A) after the bar migrated offshore from this location. The vertical mixing was generally high at the offshore station because of convective mixing throughout the experimental period.

## Discussion

The present article describes spring thermal bar circulation, its effect in inhibiting the horizontal mixing, and spatial and temporal variability of vertical mixing during this period. The theoretical framework created for the thermal bar circulation in large dimictic lakes provides the general characteristics of density-induced circulation. The primary density-induced horizontal circulation is counterclockwise circulation in the stably stratified nearshore region and clockwise in the offshore region. The secondary circulation associated with the thermal bar, perpendicular to the primary circulation, consists of two circulation cells, one on each side of the thermal bar, where waters mix and descend. The limited observational evidence of temperature and currents somewhat supported this hypothesis (Malm et al. 1993;

Gbah and Murthy 1998). However, the field investigations so far have been either confined to a few surveys or limited to observations at a particular depth. We used several ADCPs and thermistor moorings in conjunction with weekly survey data, which provided a clear description of the flow regime and turbulent exchange characteristics during spring 2003 in Lake Ontario.

The observed circulation within a zone between the shore and the thermal bar was predominantly parallel to shore and toward the west (i.e., counterclockwise). The flow away from the thermal bar to offshore showed clockwise circulation on a few occasions. The coastal circulation was mainly influenced by the alongshore winds. One of the interesting observations in this experiment is that the thermal bar was stationary for several days. Although mean cross-shore flow reduced during the thermal bar, it appears that it is depth dependent. In general, the theoretical models overestimated the progression rate of the thermal bar during the early phase. In the later phase, the model that incorporated the effect of horizontal heat flux in the thermal bar region was able to predict the significant increase in the progression rate. The calculations clearly indicate the possibility of heat advection from warm nearshore areas to the thermal bar. The effect of wind on the thermal bar seems to be an important feature, and models have to incorporate this effect. Recently, Farrow and McDonald (2002) suggested that inertial oscillations generated during the thermal bar period will influence the propagation speed of the thermal bar. The temporal distributions of temperature in both shallow and deep waters (Fig. 4a–d) did not show indications of inertial oscillations (~17.34 h) before the thermal bar period; however, during the post-thermal bar period, under stable stratification, inertial oscillations were generated. However, the band-pass filtered (14–18 h) currents showed the generation of inertial oscillations (1–3 cm s<sup>-1</sup>) caused by strong wind events, even when the water temperatures were <4°C (figures not shown). Therefore, the predictions of the thermal bar progression can be improved further by considering the role of variable wind stress and the Earth's rotation in the models.

The horizontal turbulent exchange parameters showed nonisotropic conditions in the shallow stably stratified region. The alongshore horizontal exchange coefficients were higher than cross-shore exchange coefficients. During the thermal bar period, the magnitude of both alongshore and cross-shore exchange coefficients decreased when the bar was still within middepth (<40 m). In contrast to an earlier study (Gbah and Murthy 1998), from middepth onward, the thermal bar did not show any effect on alongshore exchange coefficients, but cross-shore exchanges decreased marginally. Although this supports the hypothesis that the thermal bar plays an important role in suppressing horizontal mixing in the shallow depths, its effect was not that significant in deep offshore areas. The lateral current shear between the nearshore and the thermal bar region could be an important factor in maintaining horizontal exchanges in the deeper waters.

Vertical exchange coefficients closely relate to the dynamic stability of the water column. In general,  $K_z$  values varied significantly from the nearshore stably stratified areas to offshore areas. The vertical exchange coefficients observed dur-

ing the thermal bar were comparable to the high values observed during significant upwelling episodes in Lake Ontario (Rao and Murthy 2001). The high values in the water column were due to the convective mixing during the thermal bar. During the evolution of the spring thermal bar, vertical mixing decreased considerably in the nearshore regions under stable stratification, whereas high vertical mixing levels continued in the offshore region for a longer period.

The physical limnological processes described in this study show that the thermal bar circulation will have an effect on the distribution of dissolved and suspended material within the nearshore zone. Spring runoff, which is enriched with chlorides and nutrients, will most likely be advected by strong alongshore currents, because the transport perpendicular to the coastline is extremely limited. Also, the descending water column mixes substances vertically, potentially delaying their flushing to the deeper parts of the lake. The water chemistry data (not shown) showed that the concentrations of nutrients and chloride were higher inshore versus offshore of the thermal bar. Further studies using nonlinear numerical models to investigate the trapping of nutrients derived from land discharges are in progress.

## References

- BENNETT, J. R. 1971. Thermally driven lake currents during the spring and fall transition periods. *Proc. Conf. Great Lakes Res.* **14**: 535–544.
- BOTTE, V., AND A. KAY. 2000. A numerical study of plankton population dynamics in a deep lake during the passage of the spring thermal bar. *J. Mar. Syst.* **26**: 367–386.
- CHEN, C. T. A., AND F. J. MILLERO. 1986. Precise thermodynamic properties for natural waters covering only the limnological range. *Limnol. Oceanogr.* **31**: 657–662.
- CSANADY, G. T. 1974. Spring thermocline behavior in Lake Ontario during IFYGL. *J. Phys. Oceanogr.* **4**: 425–445.
- DAVIES, J. A., W. M. SCHERTZER, AND M. NUNEZ. 1975. Estimating global solar radiation. *Boundary Layer Meteorol.* **9**: 33–52.
- ELLIOTT, G. H. 1971. A mathematical study of the thermal bar. *Proc. Conf. Great Lakes Res.* **14**: 545–554.
- , AND J. A. ELLIOTT. 1970. Laboratory study of the thermal bar. *Proc. Conf. Great Lakes Res.* **13**: 413–418.
- FARROW, D. E. 1995. A numerical model of the hydrodynamics of the thermal bar. *J. Fluid. Mech.* **303**: 279–295.
- . 2002. A model of the thermal bar in the rotating frame including vertically non-uniform heating. *Environ. Fluid Mech.* **2**: 197–218.
- , AND N. R. McDONALD. 2002. Coriolis effects and the thermal bar. *J. Geophys. Res.* **107**: C5.
- GBAH, M. B., S. J. JACOBS, G. A. MEADOWS, AND A. BRAKTOVICH. 1998. A model of the thermal bar circulation in a long basin. *J. Geophys. Res.* **103**: 12807–12821.
- , AND C. R. MURTHY. 1998. Characteristics of turbulent cross and alongshore momentum exchanges during a thermal bar episode in Lake Ontario. *Nord. Hydrol.* **29**: 57–72.
- HUANG, J. C. K. 1972. The thermal bar. *Geophys. Fluid Dyn.* **3**: 1–28.
- KREYMAN, K. D. 1989. Thermal bar based on laboratory experiments. *Oceanology* **29**: 695–697.
- MALM, J. 1995. Spring circulation associated with the thermal bar in large temperate lakes. *Nord. Hydrol.* **26**: 331–358.
- , D. MIRONOV, A. TERZHEVIK, AND L. GRAHN. 1993. Field

- investigation of the thermal bar in Lake Ladoga—spring 1991. *Nord. Hydrol.* **24**: 339–358.
- , ———, ———, AND L. JÖNSSON. 1994. Investigation of the spring thermal regime in Lake Ladoga using field and satellite data. *Limnol. Oceanogr.* **39**: 1333–1348.
- MOLL, R. A., A. BRAKTKOVICH, W. Y. B. CHANG, AND P. PU. 1993. Physical, chemical and biological conditions associated with the early stages of the Lake Michigan vernal thermal front. *Estuaries* **16**: 92–103.
- PACANOWSKI, R. C., AND S. G. PHILANDER. 1981. Parameterization of vertical mixing in numerical models of tropical oceans. *J. Phys. Oceanogr.* **11**: 1443–1451.
- RAO, Y. R., AND C. R. MURTHY. 2001. Nearshore currents and turbulent exchange characteristics during upwelling and downwelling events in Lake Ontario. *J. Geophys. Res.* **106**: 2667–2678.
- RODGERS, G. K. 1968. Heat advection within Lake Ontario in spring and surface water transparency associated with the thermal bar. *Proc. Conf. Great Lakes Res.* **1**: 942–950.
- . 1971. Field investigation on the thermal bar in Lake Ontario: Precision measurements. *Proc. Conf. Great Lakes Res.* **14**: 618–624.
- SCAVIA, D., AND J. R. BENNET. 1980. Spring transition in Lake Ontario: A numerical study of the causes of the large biological and chemical gradients. *Can. J. Fish. Aquat. Sci.* **37**: 823–833.
- SCHERTZER, W. M. 1987. Heat balance and heat storage estimates for Lake Erie, 1967 to 1982. *J. Great Lakes Res.* **13**: 454–467.
- TAYLOR, G. I. 1921. Diffusion by continuous movements. *Proc. Lond. Math. Soc.* **20**: 196–212.
- THIKHOMIROV, A. I. 1963. The thermal bar of Lake Ladoga, *Bull. (Izvestia) All-Union Geogr. Soc.* **95**: 134–142.
- ZILITINKEVICH, S. S., K. D. KREIMANN, AND A. Y. TERZHEVIK. 1992. The thermal bar. *J. Fluid Mech.* **236**: 27–42.

*Received: 11 February 2004*

*Accepted: 22 June 2004*

*Amended: 12 July 2004*